

Surface Micromachined Devices for Microwave and Photonic Applications

M. Frank Chang and Ming C. Wu

Electrical Engineering Department
University of California, Los Angeles
Los Angeles, California 90095-1594

J. Jason Yao and M. Edward Motamedi

Rockwell Science Center
1049 Camino Dos Rios
Thousand oaks, California 91360

ABSTRACT

As an enabling technology, Micro Electro Mechanical Systems (MEMS) have continuously provided new and improved design/implementation paradigms for a variety of scientific and engineering applications. In this paper, we review recent advances made in MEMS and its derivative MOEM (Micro Opto Electro Mechanical) devices for both microwave and photonic applications.

In the area of microwave, the MEMS switch has been regarded as one of the most crucial components. The developed switch uses a suspended silicon dioxide micro-beam as the cantilever arm, a platinum-to-gold electrical contact, and electrostatic actuation as the switching mechanism. It functions from DC to microwave frequencies and has an excellent electrical isolation (>-50 dB at 4GHz and >-25 dB at 40 GHz) and minimum insertion loss (< 0.1 dB at 4 GHz and < 0.5 dB at 40 GHz). Compared to its semiconductor counterparts, the MEMS switch is superior in both performance and power consumption.

In the area of photonics, the microoptical components, such as diffractive and refractive microlenses, micromirrors, beam splitter and beam combiners have received considerable attention recently. Optical systems that once were considered to be impractical due to the limitations of bulk optics can now easily be designed and fabricated with all required optical paths, signal conditioning, and electronic controls, integrated on a single chip. On-chip optical processing will enhance the performance of devices such as focal plane optical concentrators, beam shapers, Fiber Data Distribution Interface (FDDI) switch, and miniature tunable 3-D Fabry-Perot Etalon. In this paper we review advances in MEMS switches and microoptical components developed at the Rockwell Science Center. We also review the potential of on-chip optical processing and the recent achievement of free-space integrated optics and microoptical bench components developed at UCLA.

Keywords: MEMS, microwave swtches, microoptics, MOEM, actuators, integration, mirror, microlens, FDDI, and 3-D Fary-Perot.

1. INTRODUCTION

The continuous growth of MEMS has offered paradigm shifts in miniature device design for a variety of scientific and industrial applications. Two major application areas will be addressed in this paper: the microwave MEMS switches and photonic MEOM devices. Switches are widely used in microwave systems and subsystems for signal routing, impedance matching, and amplifier gain adjustment. Traditional solid state switches have a significant insertion loss (typically >1 dB) in

the 'On' state and a poor isolation (typically < -30 dB) in the 'Off' state even at low microwave frequencies (about 1 GHz)¹. Here we describe the design, fabrication and performance of a MEMS switch which can handle broadband microwave signals (up to 40 GHz), while maintaining a minimal insertion loss and an excellent electrical isolation.

On the other hand, microoptical components, such as diffractive and refractive microlenses, have recently received considerable attention for the development of optical systems³. In the first generation of the miniaturized optical system, microoptical components were hybridized with electronics circuits and in some cases with movable components such as scanning mirrors and piezo-actuators. As the MEM and MOEM technologies continue to advance, miniaturized optical systems may also advance to nearly monolithic systems. Integrated devices based on MOEM systems can form free space integrated optics and consequently push technology to the development of a microoptical bench-on-a-chip.

2. MICROWAVE SWITCH

2.1 Switch Design

The MEMS switch is designed for applications with signal frequencies from DC to 40 GHz. Figure 1 shows a schematic illustration of a surface micromachined switch design. Figure 2 contains a topview micrograph of a fabricated MEMS switch.

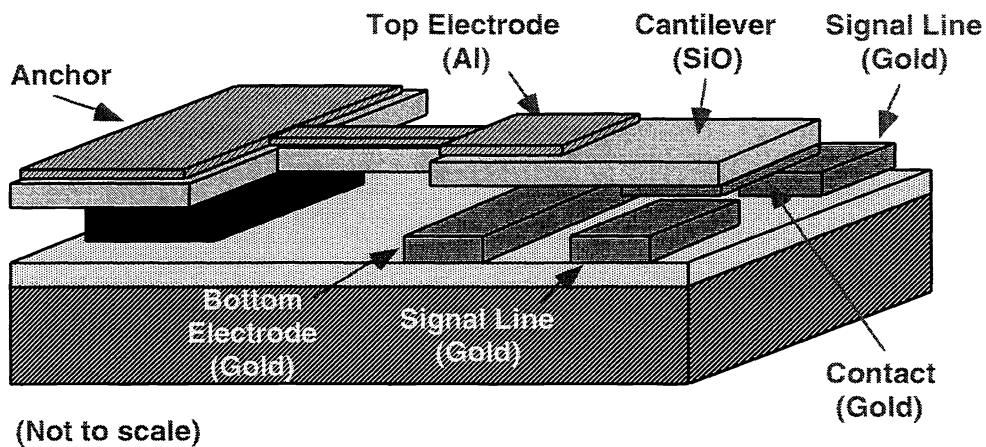


Fig.1 A schematic illustration of a micromachined RF switch design

As shown in Fig.1, for the general design of the MEMS switches, the silicon dioxide cantilevers are typically between 100 μm and 200 μm in length, 10 μm in width, and 2 μm thick. The grid capacitor structures in Fig. 2 have an overall area of 200 μm by 200 μm . The gap between the bottom of the silicon dioxide cantilever and the metal lines on the substrate is 3 μm . The gold microstrip signal lines are 2 μm thick, and between 20 μm and 40 μm in width. The gold contact metal is 1 μm thick. The contact area is on average 400 μm^2 .

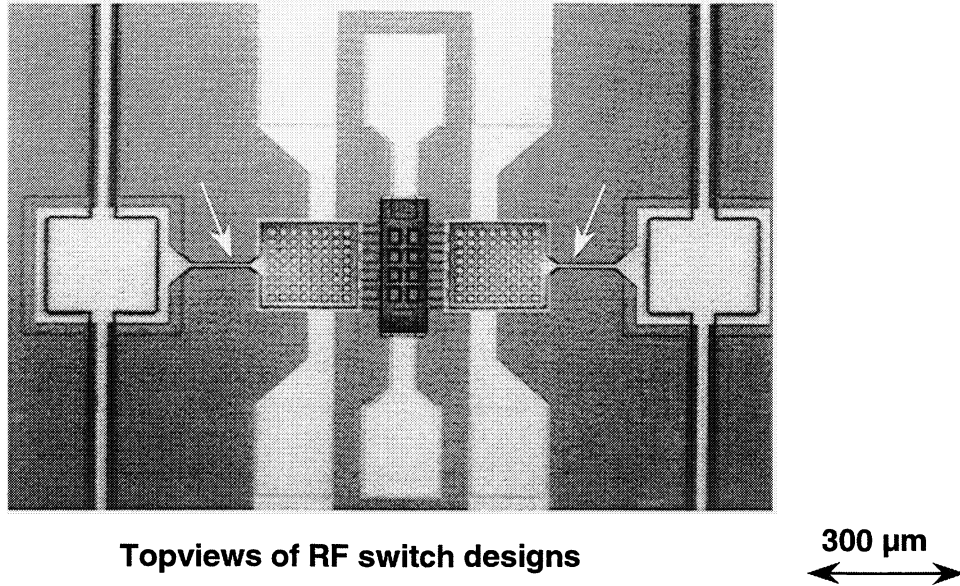


Fig. 2: Micrograph image showing the topview of a fabricated RF switch.

At low RF frequencies, the insertion loss is dominated by the resistive loss of the signal line which includes the resistance of the signal line and the contact resistance. At higher frequencies, the insertion loss can be attributed to both the resistive loss and the skin depth effect. To minimize the resistive loss, a thick layer ($2\ \mu\text{m}$) of gold is used. The width of the signal line is a more limited variable than the thickness because the wider the line, the lower the insertion loss, but also the poorer the 'Off' state electrical isolation due to the increased line capacitance. Electrical isolation of the switch also depends on the capacitive coupling between signal lines and the substrate. Therefore, the semi-insulating GaAs substrate is chosen for the RF switch over a conductive silicon substrate. GaAs substrates are used instead of other insulating substrates such as glass so that the RF switch may retain its monolithic integration capability with MMICs.

The capacitive coupling between signal lines may be reduced by increasing the gap between the signal lines on the substrate and the gold contact metal on the bottom of the suspended silicon dioxide cantilever (Fig. 1). However, this increase in the gap also increases the voltage required to actuate the switch because the gap distance also determines the actuation capacitance. The aluminum top metal of the capacitive actuator couples to the underlying gold ground (GND) metallization across this gap. For a fixed gap distance, the voltage required to actuate the switch may be reduced by increasing the actuation capacitor area. However, this increase in the capacitor area increases the overall mass of the suspended structure and thus the closure time of the switch. If the stiffness of the suspended structure is increased to compensate the increase in the structure mass to maintain a constant switch closure time, the required voltage to actuate the switch will be further increased.

In managing the tradeoffs between the device parameters for the applications in which the RF switches will be used, the insertion loss and the electrical isolation are given the highest priority, followed by the closure time, and finally the actuation voltage. The grids in the actuation capacitor structure introduced in the designs shown in Fig. 2 reduce the structural mass while maintaining the overall actuation capacitance by relying on the fringing electric fields of the grid structures. A second reason for the use of the grid structures is to reduce the atmospheric squeeze damping between the cantilevered paddles and the substrate. Switches without the grid design were observed to have a much larger closure and opening time due to the squeeze damping effect.

2.2 Switch Fabrication

The RF switches are manufactured using a surface micromachining technique with a total of five masking levels². PECVD silicon dioxide is deposited as the structural material, and polyimide is used as the sacrificial material. Figure 3 is a cross-

sectional schematic illustration of the process sequence. The low process temperature budget of 250°C ensures the switch's monolithic integration capability with MMICs. Starting from a 3-inch semi-insulating GaAs wafer, a layer of thermal setting polyimide (DuPont PI2556) is spun on and cured via a sequence of oven bakes with the highest baking temperature of 250°C. A layer of pre-imidized polyimide (OCG Probimide 285) is then spun on and baked with the highest baking temperature of 170°C. A silicon nitride layer 1500 Å thick is then deposited and patterned using photolithography and reactive ion etched (RIE) in CHF₃ and O₂ plasma. The pattern is further transferred to the underlying polyimide layers via O₂ RIE (Fig. 3a). This creates a liftoff profile similar to the tri-layer resist system except that two layers of polyimide are used. A layer of gold is electron beam evaporated with a thickness equal to that of the thermal set DuPont polyimide layer. The gold liftoff is completed using methylene chloride to dissolve the pre-imidized OCG polyimide, leaving a planar gold/polyimide surface (Fig. 3b). The cross linked DuPont polyimide has good chemical resistance to methylene chloride.

A second layer of thermal setting polyimide (DuPont PI2555) is spun on and thermally cross linked. A layer of 1 μm gold is deposited using electron beam evaporation and liftoff to form the contact metal (Fig. 3c). A 2 μm thick layer of PECVD silicon dioxide film is then deposited and patterned using photolithography and RIE in CHF₃ and O₂ chemistry (Fig. 3d). A thin layer (2500 Å) of aluminum film is then deposited using electron beam evaporation and liftoff to form the top electrode in the actuation capacitor structure (Fig. 3e). And lastly, the entire RF switch structure is released by dry etching of the polyimide film in a Branson O₂ barrel etcher. The dry-release is preferred over wet chemical releasing methods to prevent any potential sticking problems during release.

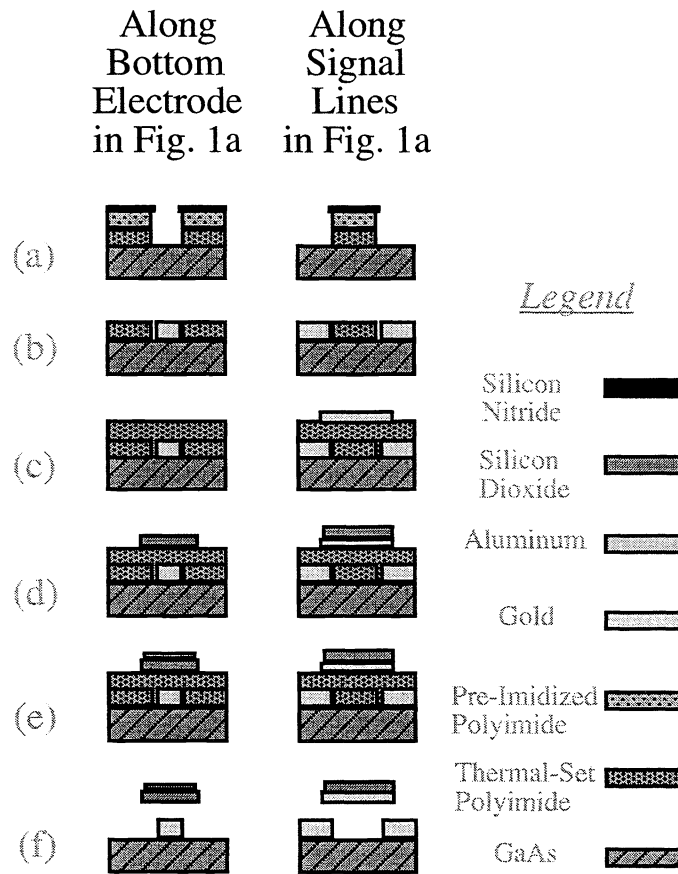
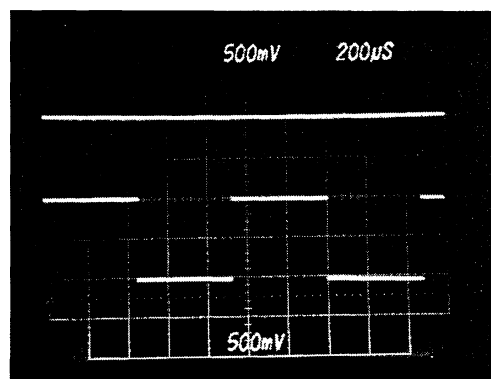


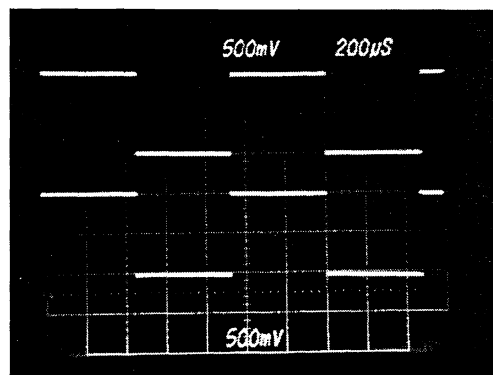
Fig. 3 An abbreviated schematic illustration of the RF switch process sequence.

2.3 Microwave performance of MEMS switches

The stiffness of the suspended switch structure is designed to be between 0.2 N/m and 2.0 N/m for various cantilever dimensions. The lowest required actuation voltage is 28 Volts with an actuation current on the order of 50 nA which corresponds to a power consumption of 1.4 μ W. It requires zero power to maintain the switch in either the 'On' or 'Off' state due to the nature of the electrostatic actuation. The switch closure time is on the order of 10 μ s. All characterization was performed in an atmospheric ambient. The silicon dioxide cantilever has been stress tested for a total of sixty five billion cycles (6.5×10^{10}), and no fatigue problem was observed. The maximum current handling capability for the prototype switch is 200 mA with the cross sectional dimensions of the narrowest gold signal line being 1 μ m x 20 μ m. Figure 4 shows the low frequency (1 kHz) input and output response of the RF switch in the 'On' and 'Off' states. As shown in Fig.5, an electrical isolation of -50 dB and an insertion loss of 0.1 dB at 4 GHz have been achieved. When tested at 40 GHz, the MEMS switch showed an insertion loss of 0.5 dB and the isolation of -25 dB. At both frequencies, the MEMS switch has outperformed traditional semiconductor switches at least 10 dB in isolation and 1-2 dB in insertion loss.



Switch in the 'Off'



Switch in the 'On'

Input: 1V pp @ 1 KHz

Fig. 4 The switch output response in the (a) 'Off' and (b) 'On' states to a 1 Volt input signal at 1 kHz.

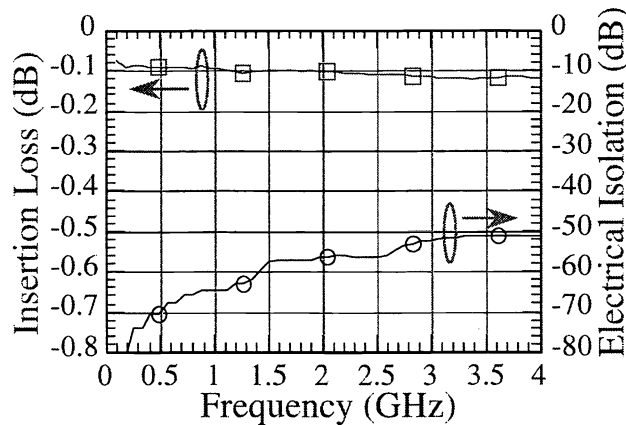


Fig. 5 Insertion loss and isolation of the RF switch from 100 MHz up to 4 GHz.

3. MICROOPTICS

Microoptics technology is becoming increasingly essential to the development of many optical systems. Optical components such as diffractive and refractive microlens, multilevel optical gratings, and beam splitters are being incorporated into advanced sensor systems. Microoptics is an enabling technology for applications that cannot be addressed using conventional optics. In the following we will discuss some of these microcomponents.

3.1 Diffractive microlens

A diffractive microlens is a microoptical component as small as a few tens of a micron in diameter and with a thickness on the order of an optical wavelength. The microlens speed can be as fast as $f/0.3$ in air for high index materials such as silicon and GaAs and about $f/1$ for quartz and glass substrates. A diffractive microlens is an approximation of a kinoform, or continuous diffractive lens. The kinoform lens structure can be approximated by multilevel lithography and stepwise etching. To fabricate a multistep process, binary optic design is considered Fig. 6. Binary optics will reduce the number of lithographic masks by a factor of $2^m/m$, where m is the number of required masks.

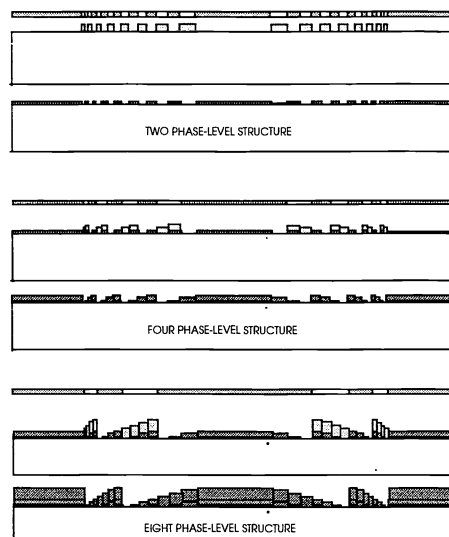


Fig. 6 shows a processing cycle for fabrication of an eight-level binary optic microlens. Fig. 6(a), 6(b) and 6(c) illustrate the process of two-phase, four-phase and eight-phase microlenses⁵.

The spectral range of short wave infrared (SWIR) focal plane arrays (FPAs) is from 1.5–2.5 μm . These arrays have numerous applications in medicine, security, industrial inspection, and IR astronomy, all of which will benefit from diffractive optics. High sensitivity at high operating temperature is often important in these applications. Conventional FPAs have relatively poor sensitivity and low signal-to-noise ratio at high temperatures. Integrating binary optic microlenses and hybrid FPA technologies leads to a new approach to reduce detector size, while retaining a given image resolution and optical collection area. The resultant detector volume reduction has led to a significant decrease in detector dark current and, hence, to an increase in device performance.

Recent results from Rockwell⁴ show that integration of microoptics and SWIR HgCdTe can produce detectors that perform exceptionally at elevated operating temperatures. The detector configuration of this effort is shown in Fig. 7. Here light incident on the backside of the substrate is focused by a thin film binary optic into the detector forming total internal reflection; the mesa sides augment the diodes' light-gathering abilities beyond the physical extent of the active layer. Note that with no buffer layer, delineation of the active area is incomplete, and the effective optical area of the detector will be wavelength dependent due to shorter wavelengths being more effectively absorbed by the mesa valleys which have larger area. Retaining the planar geometry on top of the mesa preserves the passivation advantage of the cap layer and as a result enhances the optical efficiency of the system.

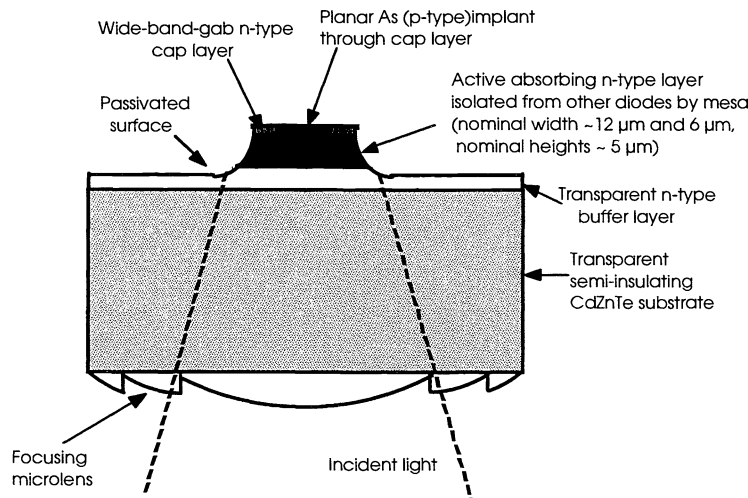


Fig.7 Planar mesa architecture, demonstrating the potential for integration of microlens with FPA.

3.2 Refractive microlenses

Refractive microlenses may provide an attractive, low-cost alternative to diffractive microlenses. Refractive and diffractive microlenses are complementary, and in some cases refractive optics is a sole solution to optical system design. For example, in the case of a short wavelength optical system ($\lambda < 1 \mu\text{m}$) requiring high speed microlenses ($< f/4$), diffractive optics faces process limitation ($CD < 1 \mu\text{m}$). At Rockwell, we have designed and fabricated refractive microlenses by RIE and ion milling, in fused quartz, bulk silicon, CdTe, GaAs, InP, and GaP; and by thin film deposition of Ge films on fused silica and Al_2O_3 . Lens diameters ranged from 30 to 500 μm , and lens f numbers were in the range of $f/0.76$ – $f/6$.

Reliable and reproducible fabrication of microlens arrays depends on accurate control of photolithographic and reactive ion etching processes. Photoresist microlenses can be reliably fabricated within a range of aspect ratios. Dimensional control of microlenses in the solid material can then be tailored by carefully controlled reactive ion etching. Both mixtures of SF_6 or O_2 with CF_3H were used to accurately control the lens sag during etching. Figure 8 is a SEM micrograph of a InP microlens with speed of $f/1$, 50 μm diameter and centers spaced at 70 μm .

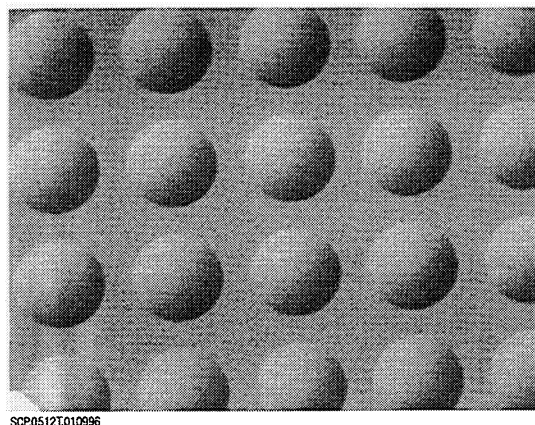


Fig.8 SEM micrograph of an $f/1$, 50- μm -diam linear microlens array fabricated in InP.

4. MICROOPTICAL MEMS: MOEM SYSTEMS

Micromachining of silicon substrate has been applied to integrated optics and the realization of a miniature optical bench. Also, surface micromachined hinges and spring-latches⁵ have been used to achieve monolithic fabrication of three-dimensional micro-optics.⁶ This technology opens a new area for integrated optics in free space. Using this new technique, three-dimensional micro-optical components can be fabricated integrally on a single Si chip. The Si substrate serves as a micro-optical bench on which microlenses, mirrors, gratings and other optical components are prealigned in the mask layout stage using computer-aided design and then constructed by microfabrication. Additional fine adjustment can be achieved by the on-chip micro-actuators and micropositioners, such as rotational and translational stages. With hybrid integration of active optical devices, a complete optical system can be constructed, as illustrated in Fig.9.

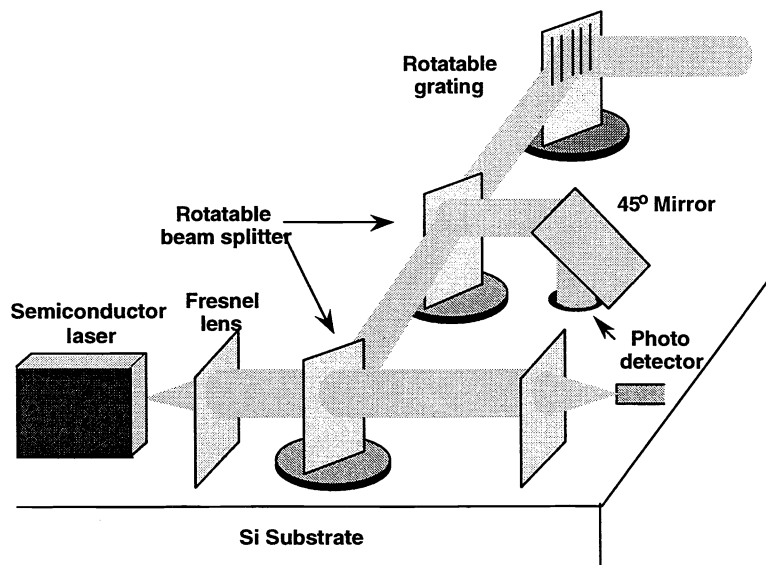


Fig.9 The schematic diagram illustrating the micromachined free-space micro-optical system on a single substrate

4.1 Microbase, micromount, and microhinge design

The micro-optics plates used for mirror, beam splitter, microlens array, grating, and collimator are processed by surface micromachining, and they are released from the substrate by selectively removing the sacrificial material (deposited SiO_2)

using hydrofluoric acid after fabrication. After the release etching, the poly-plates with microoptics patterns are free to rotate around hinge pins (Fig.10). When the plate is lifted up, the top portion of the spring-latch slides into a slot on the plate, and snaps into a narrower part of the slot, thus preventing further motion of the plates. The torsion-spring connecting the spring-latch to the substrate creates the spring force, which tends to force the spring-latch back to the substrate, therefore locking the plate in its place. The length of the spring latch defines the angle between the plate and the substrate. After the three-dimensional micro-optical element is assembled, a layer of gold is coated on the lifted poly surfaces. In binary-amplitude Fresnel zone plates or micro-mirrors, a thick layer of gold is needed to completely block the light passing through the dark zones or to make a perfectly reflecting mirror. On the other hand, thinner gold is desired for partially transmitting mirrors or beam splitters.

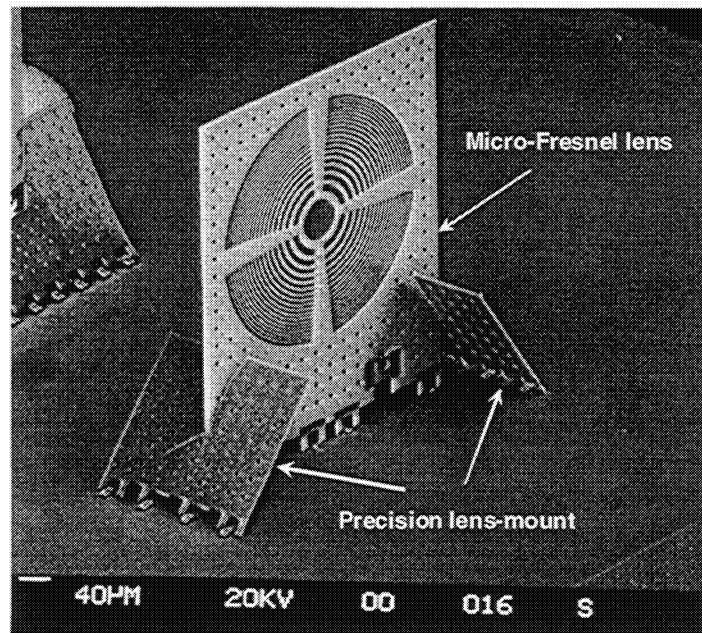


Fig.10 SEM photograph of a Fresnel microlens with precision lens mount

4.2 Fresnel microlenses

Figure 11 shows a SEM photograph of a three-dimensional Fresnel micro lens after assembly. The diameter of this lens is 280 μm , with a designed optical axis of 254 μm for passive integration of an edge-emitting semiconductor laser. The optical performance of the three-dimensional Fresnel microlens has been tested by collimating a divergent beam emitted from a single mode fiber at $\lambda = 1.3 \mu\text{m}$. The intensity FWHM divergence angle is reduced from 5.0° to 0.33° by the lens. The collimated beam profile fits the Gaussian shape (95% fit) very well.

4.3 Translation stage

One unique feature of implementing a micro-optical bench using surface micromachining is that micropositioners and microactuators can be monolithically integrated in the same fabrication processes for different types of optical translators. This allows the alignment of the optical systems to be fine adjusted, in addition to the coarse alignment done at the design stage using CAD layout tools. UCLA researchers have successfully integrated the three-dimensional micro-optical elements with rotational stages using this process. Figure 10 shows a SEM photograph of a rotatable mirror. The rotatable plate is fabricated on the first polysilicon layer, and the axis and hub are defined on the second polysilicon layer. The indicator on the lower part of the picture, originally pointing at the 0° tick, has been rotated counterclockwise by 20° after the mirror was assembled, as shown on the picture. A diffraction grating integrated with the rotational stage has been successfully demonstrated using the same technology, as shown in Fig. 11.

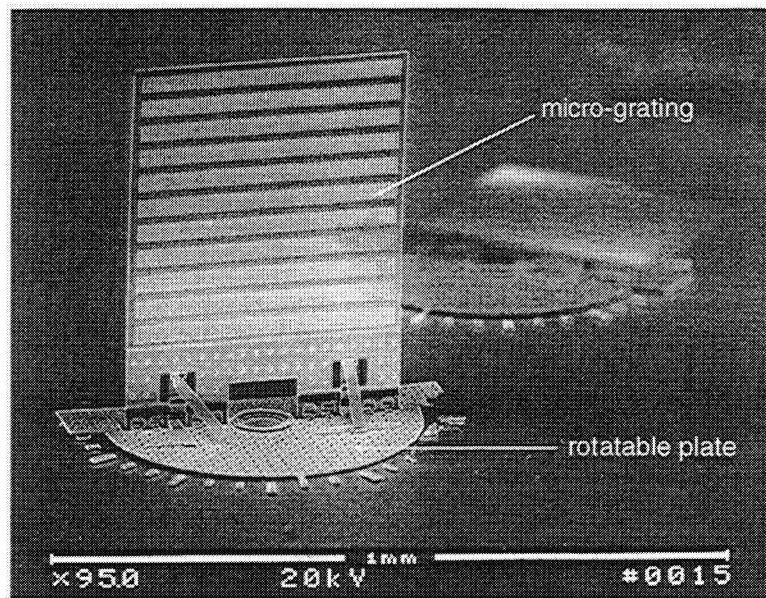


Fig.11 The diffraction grating integrated with a rotational stage

4.4 Potential applications

With the newly developed micro-bench, micro-optical components and MEMS mechanical parts, we are now ready to demonstrate their use in micro-optical systems as described as follows:

4.5 3-D Tunable Fabry-Perot

Tunable Fabry-Perot (FP) etalons are very useful for wavelength-division-multiplexed (WDM) optical communications, optical sensing, and spectral analysis applications. There has been a great deal of interest in applying the micromachining technology to realize compact tunable FP etalons, since most FP etalons are tuned mechanically. We demonstrated a novel three-dimensional tunable filter implemented on a surface-micromachined free-space microoptical bench (FS-MOB).^{7,8} It can be readily integrated with other microoptical elements (e.g., collimating and focusing lenses, or cascaded tunable filters for WDM demultiplexers) or fiber alignment V-grooves. Both parallel-plate FP etalons and solid FP etalons have been realized using FS-MOB technology.

A schematic drawing and a SEM micrograph of a solid FP etalon are shown in Fig. 12(a) and 12(b), respectively. The transmission wavelength versus the rotation angle of the etalon is shown in Fig. 13 (a). A very broad tuning range of 58.5 nm is obtained when the etalon is rotated by 70°. The experimental data agrees very well with a theoretical analysis using the transmission matrix approach. Figure 13 (b) shows the transmission spectrum of the etalon at 50° rotation. The finesse of the etalon is measured to be 11, currently limited by the scattering loss due to the granular surface of the polysilicon plate.

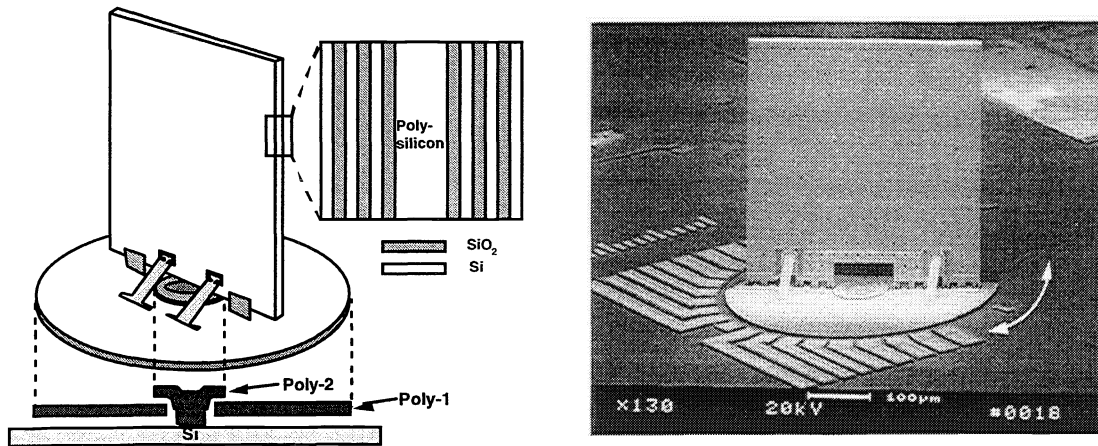


Fig.12 The schematic and SEM of the tunable solid Fabry-Perot etalon.

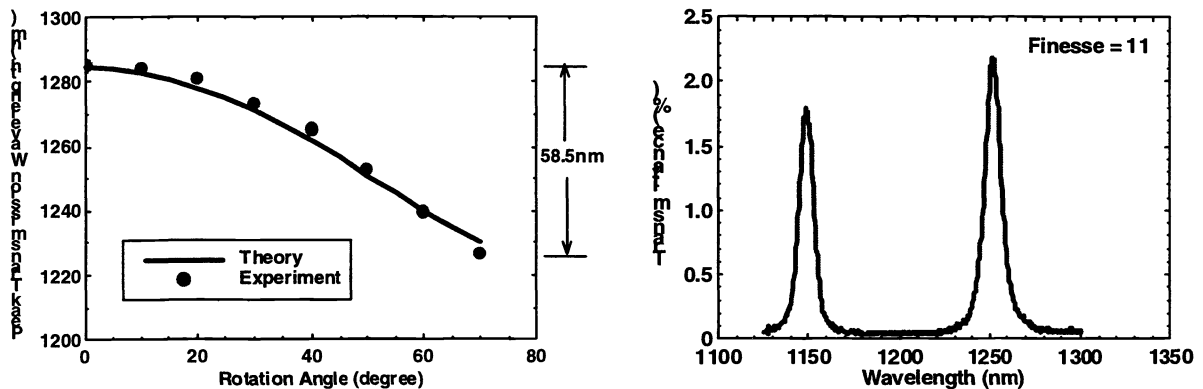


Fig.13 The wavelength tuning range and the transmission spectrum of the tunable filter

4.6 FDDI optical bypass switch

Si bulk-micromachining and wafer bonding techniques have been used to implement free-space opto-mechanical switches.⁹ However, monolithic integration is difficult and substantial assembly is still required. Here, we propose to use the surface-micromachining technology to monolithically integrate the free-space microoptical switch with microactuators and fiber optic alignment guides. They can be made compact and light weight, and are potentially integrable with optical sources/detectors and controlling electronics. The switch consists of a three-dimensional movable mirror and four optical fiber guiding rails, as shown in Fig. 14. Four multimode fibers are arranged in a “cross” configuration, with a movable micromirror placed in the center. The switch operates in two states: CROSS and BAR. When the mirror/sliding-plate is moved away from the fibers (the center), the fibers along the same diagonal directions are allowed to communicate with each other. This is defined as CROSS state. In the BAR state, the mirror/sliding-plate is slid into the center and the light signal is reflected to the orthogonal fiber.

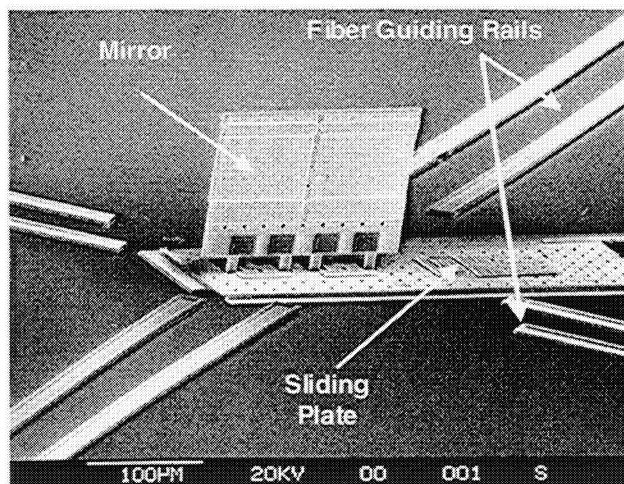


Fig. 14 The SEM of the three-dimensional mirror sitting on a sliding plate

The optical performance of the optical switch is characterized by attaching multimode fibers to the guiding rails of the optical fibers. The insertion loss of the switch for both operating states has been measured with an LED source operating at 1.3 μm wavelength. The total insertion loss of the switch has been measured to be 2.8 dB for the CROSS state and 3.1 dB for the BAR state. From these two measurements, the reflectivity of the mirror is estimated to be 93%. The crosstalk between two states is measured to be 26.1 dB. The excess loss measured here includes the Fresnel loss of the fiber (~ 0.34 dB), and possible misalignment of the fibers. Recently, the insertion losses have been reduced to 1.4 dB and 1.9 dB, respectively, with an improved design.

5. CONCLUSIONS

MEMS and MOEM technologies including both microwave and photonic devices have advanced significantly in the past several years. These technologies are anticipated to rapidly gain in maturity and become available for many microwave and photonic system applications. We have presented here a few recent developments in this emerging field and have described examples of devices that are being developed. Further significant advances can be expected for on-chip microwave and photonic processing as researchers recognize the full range of functionalities that can be realized using these exciting new technologies.

7. REFERENCES

1. Gopinath, A and Rankin, J. B. "GaAs FET RF Switches," *IEEE Tans. On Electron Dev.*, vol. ED-32, no. 7, July 1985, pp. 1272-1278. Or Kobayashi, K. W; Oki, A. K; Umemoto, D. K; Claxton, S. K. Z; and Streit, D. C. "Monolithic GaAs HBT p-I-n Diode Variable Gain Amplifiers, Attenuators, and Switches," *IEEE Trans. On Microwave Theory and Tech.*, vol. 41, no. 12, December 1993, pp. 2295-2302.
2. J.J. Yao and M.F. Chang, "A surface micromachined miniature switch for telecommunication applications with signal frequencies from DC up to 4 GHz" *Transducers '95*, pp.384-387, June, 1995.
3. M.E. Motamedi, B. Anderson, R. De La Rosa, W.J. Gunning, R.L. Hall, M. Khoshnevisan, "Binary Optics Thin Film Microlens Array", *Proceedings, SPIE*, Vol. 1544, pp. 22-32, July 1992.
4. M.E. Motamedi, W.E. Tennant, R. Melendes, N.S. Gluck, S. Park, J.M. Arias, J. Bajaj, J.G. Pasko, W.V. McLevige, M. Zandian, R.B. Hall, K.G. Steckbauer, P. D. Richardson, "FPAs and thin film binary optic microlens integration," *SPIE Proceeding of Miniature and Micro-optics and Micromechanics*, Vol. 2687, pp. 70-77, 1996. (invited paper)

5. K.S.J. Pister, M.W. Judy, S.R. Burgett, and R.S. Fearing "Microfabricated hinges", *Sensors and Actuators A*, 33, pp. 249-256, 1992.
6. L.Y. Lin, S.S. Lee, K.S.J. Pister, and M.C. Wu, "Three-dimensional Micro-Fresnel Optical Elements Fabricated," *Micromachining Technique by Electronics Letters*, Vol. 30 No. 5
7. L.Y. Lin, J.L. Shen, S.S. Lee, M.C. Wu, and A.M. Sargent, "Tunable three-dimensional solid Fabry-Perot etalons fabricated by surface-micromachining," *IEEE Photonics Tech. Lett.*, Vol. 8, no. 1, pp. 101-103, 1996.
8. J.L. Shen, L.Y. Lin, S.S. Lee, M.C. Wu, and A.M. Sargent, "Surface-micromachined tunable three-dimensional solid Fabry-Perot etalons with dielectric coatings," *Elec. Lett.*, Vol. 31, no. 25, pp. 2172-2173, 1995.
9. M.F. Dautartas, A.M. Benzoni, Y.C. Chen and G.E. Blonder, "A silicon-based moving-mirror optical switch", *J. of Lightwave Technology*, Vol. 10, No. 8, August, 1992.